Electronic Supplementary Information

A Bi-Functional pH-Responsive Chip with a Soft Hydrogel-supported 3D-like Renal Tumor Model for Sustained Drug Delivery

Upasana Gupta[1],Bisma Yousuf[2], Shashank Kumar Singh[2*], Ravi Kumar Arun[1*]

[1] Department of Chemical Engineering, Indian Institute of Technology Jammu, Jammu, Jammu and Kashmir, 181221, India

[2] Council Of Scientific And Industrial Research–Indian Institute Of Integrative Medicine, Jammu, Post Bag 3, Canal Rd, Canal Road, Jammu, Jammu and Kashmir 180001

Corresponding author:** ***Email: ravi.arun@iitjammu.ac.in, sksingh@iiim.ac.in

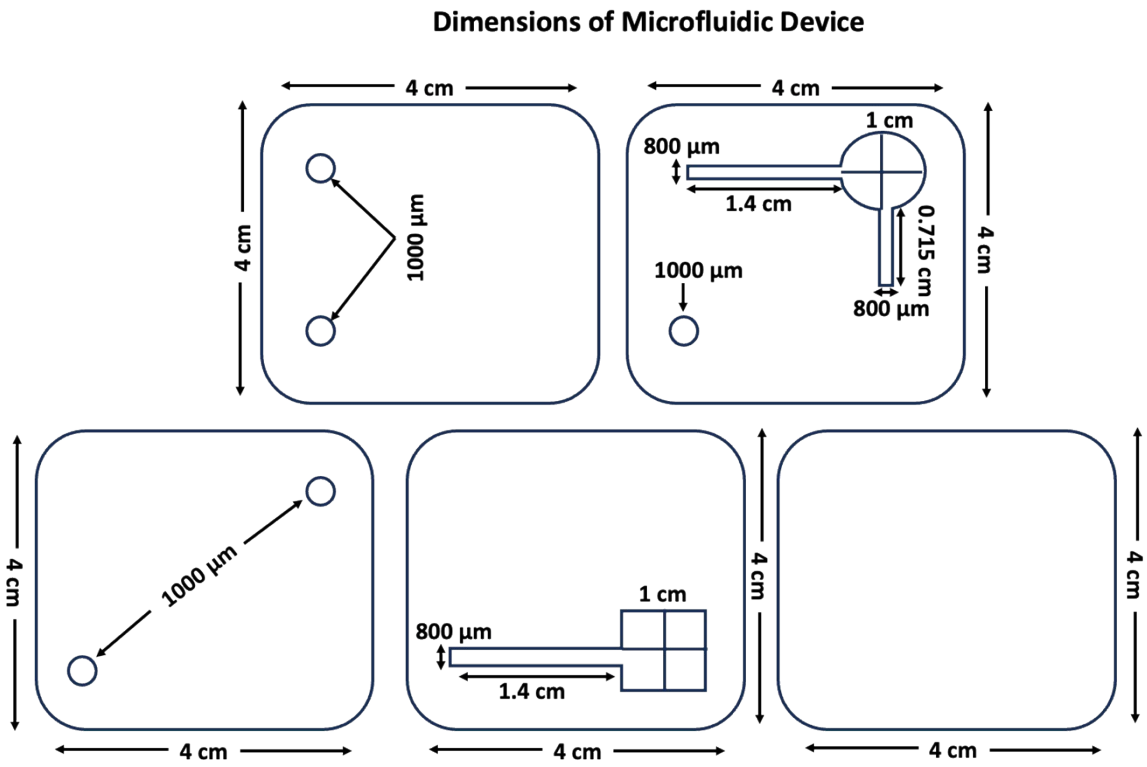

Figure S1. Schematic illustration of the PMMA-based microfluidic chip design used for hydrogel integration and cell culture. The figure shows channel geometry, inlet and outlet ports, and hydrogel chamber configuration for controlled perfusion and localized drug delivery.

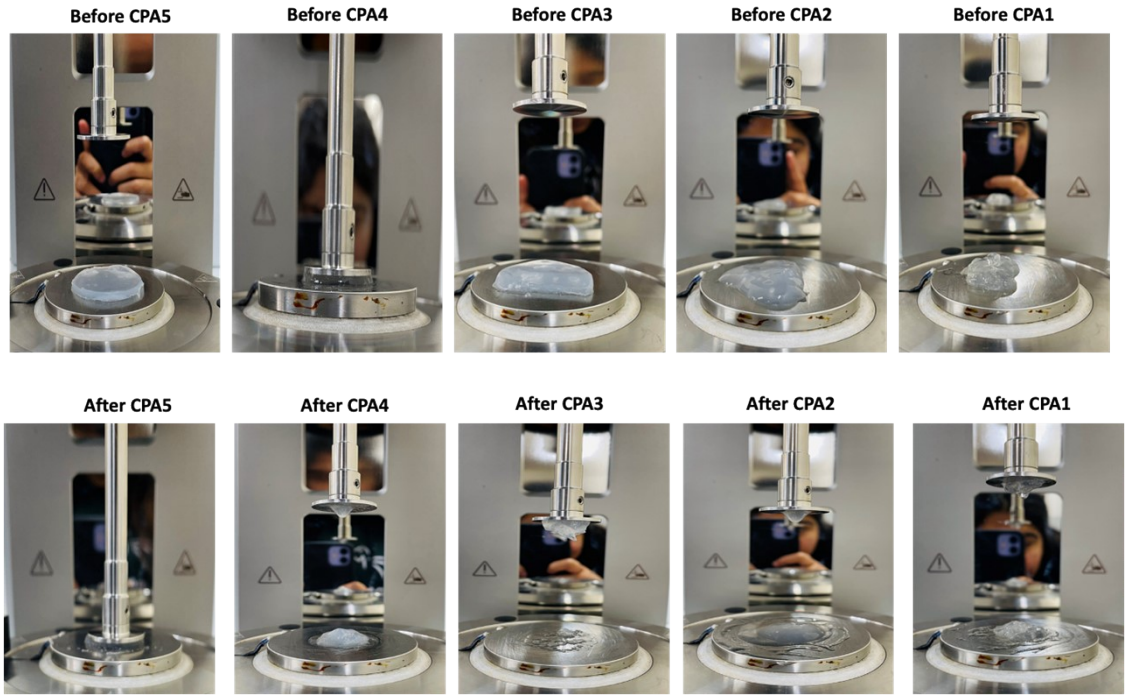

Figure S2. Sequential images showing rheological deformation and recovery of the CPA5% hydrogel under oscillatory strain during amplitude sweep testing at 37 °C using an Anton Paar MCR 702 rheometer (parallel plate geometry, 25 mm, 3 mm gap). The series illustrates the gel's compression, deformation, and relaxation behavior, confirming its viscoelastic and self-recovering characteristics.

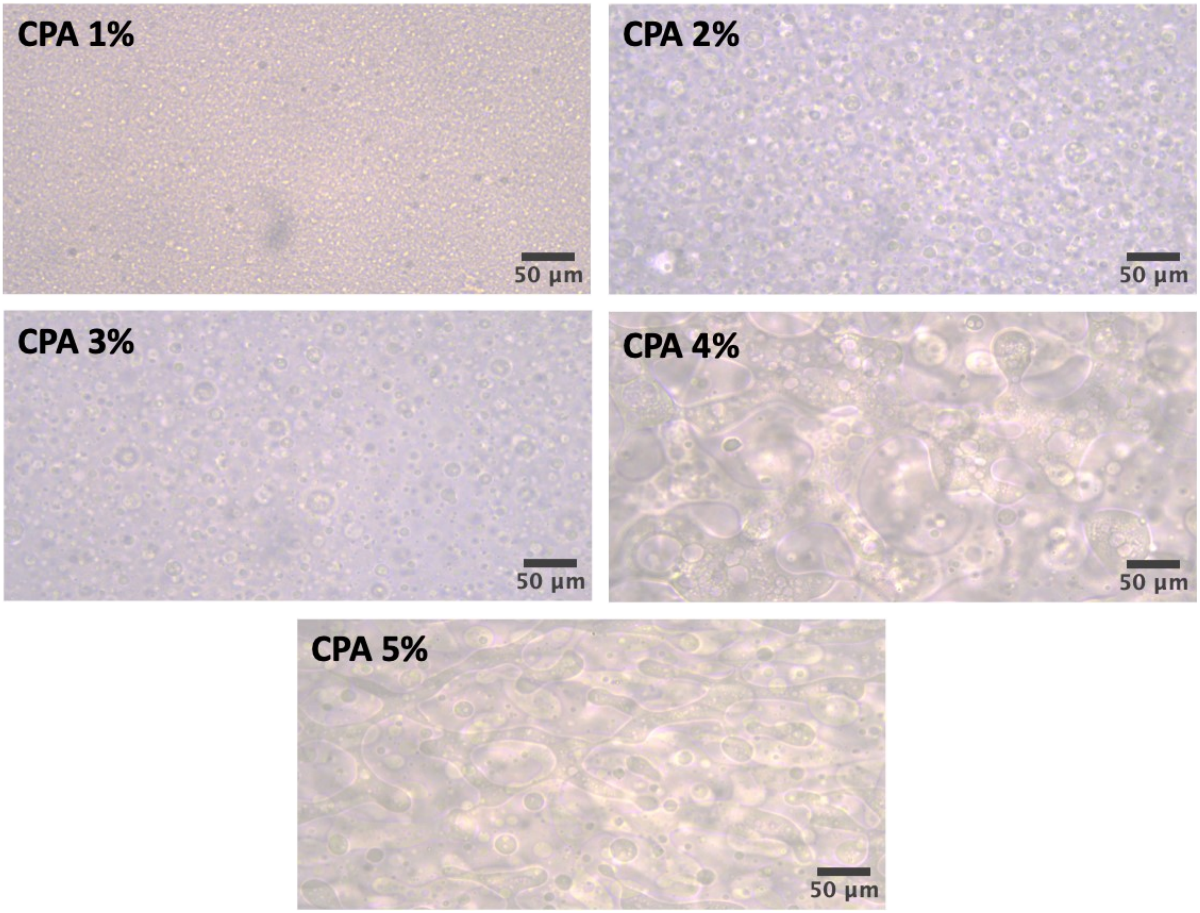

Figure S3. Optical micrographs (20× magnification) of hydrated CPA hydrogels with varying agarose concentrations (CPA1–CPA5). The pore density and network definition increased with the agarose content, with CPA4 and CPA5 exhibiting well-developed, interconnected structures characteristic of stable, hydrated hydrogel networks.

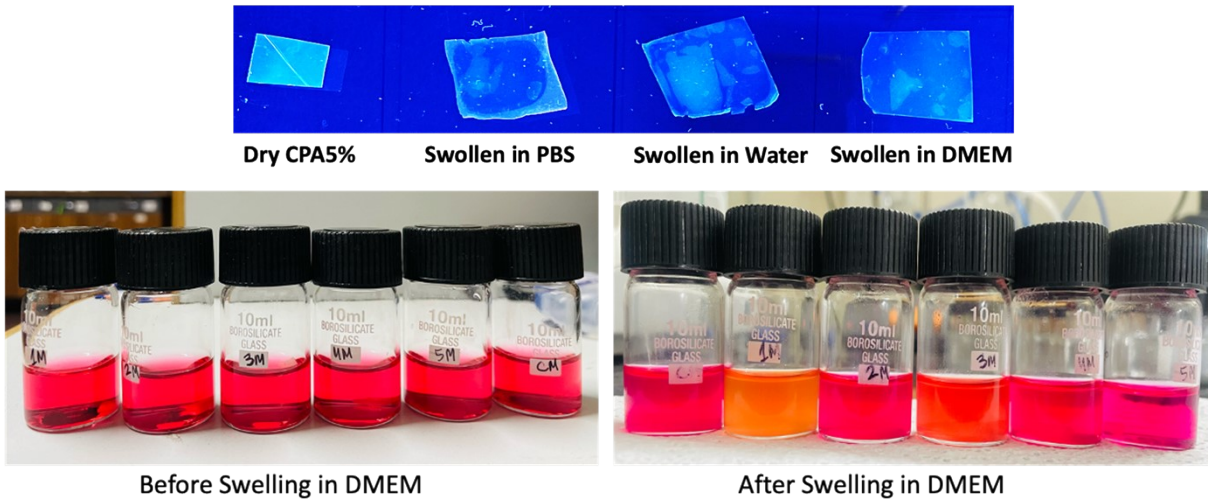

Figure S4. Swelling behavior of CPA hydrogels in different media. (Top) images of dried CPA5% hydrogels swollen in phosphate-buffered saline (PBS), deionized water, and Dulbecco's Modified Eagle Medium (DMEM), showing distinct swelling and transparency variations. (Bottom) Photographs of CPA hydrogels (CPA1–CPA5) after equilibrium swelling in DMEM at 37 °C, illustrating the effect of agarose concentration on hydration capacity and media absorption.

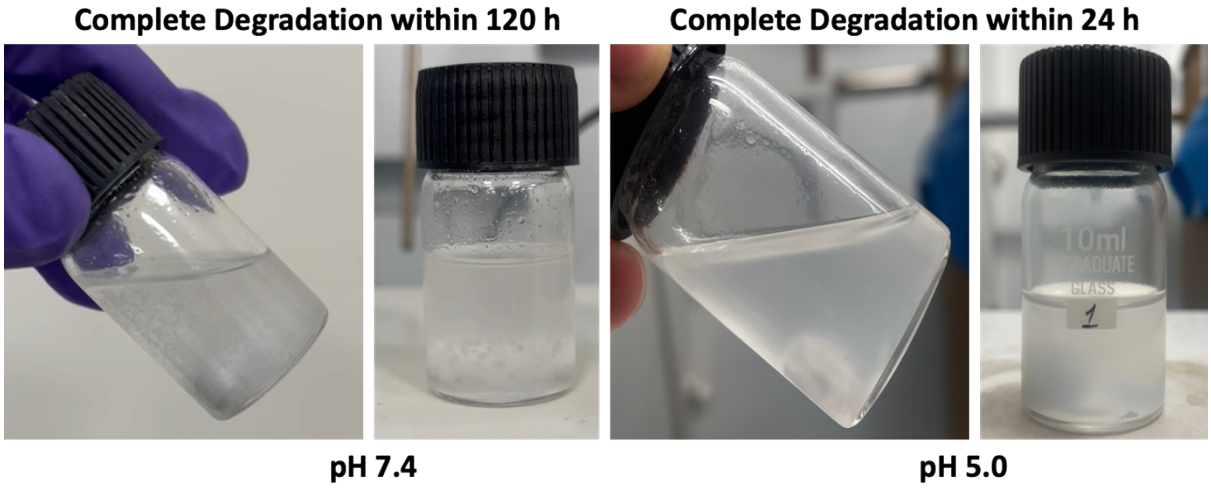

Figure S5. Degradation behavior of CPA5% hydrogels at different pH conditions. Representative photographs show the physical appearance of hydrogels incubated in phosphate-buffered saline (PBS) at pH 5.0 and pH 7.4 at 37 °C over time. The CPA5% hydrogel

took 120 h to completely degrade at pH 7.4, while at pH 5.0 it readily dissolved within 24 h and thus slowly lost its structural integrity at physiological pH (7.4), while at acidic pH (5.0), progressive disintegration and liquefaction were observed, indicating accelerated degradation due to the protonation of carboxyl groups and weakening of hydrogen-bonded cross-links.

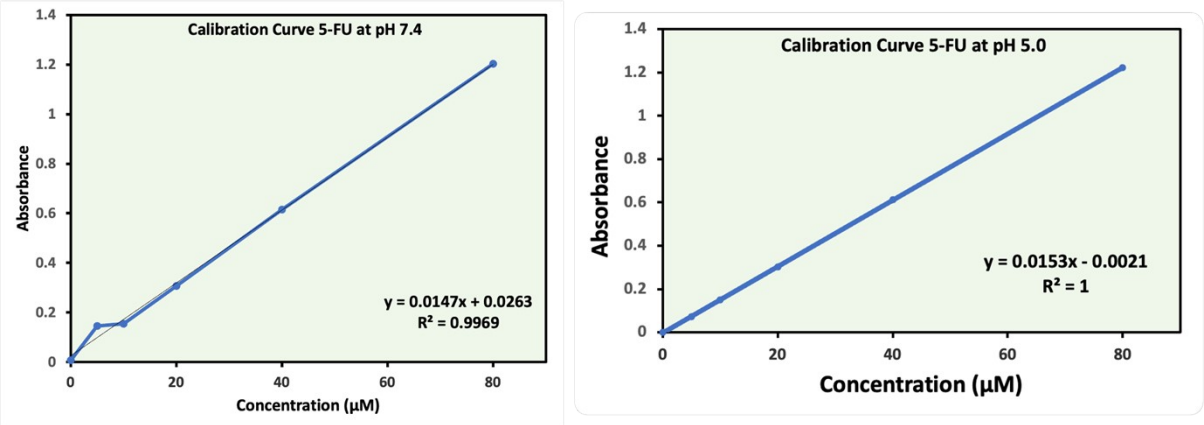

Figure S6. Calibration curves of 5-fluorouracil (5-FU) at different pH conditions. (a) Calibration curve at pH 7.4 showing linear correlation between absorbance and concentration with the regression equation y = 0.0147x + 0.0263 (R^2 = 0.9969). (b) Calibration curve at pH 5.0 with regression equation y = 0.0153x − 0.0021 (R^2 = 1). The strong linearity in both conditions confirms the reliability of UV–Vis spectrophotometric quantification of 5-FU across physiological and acidic environments.

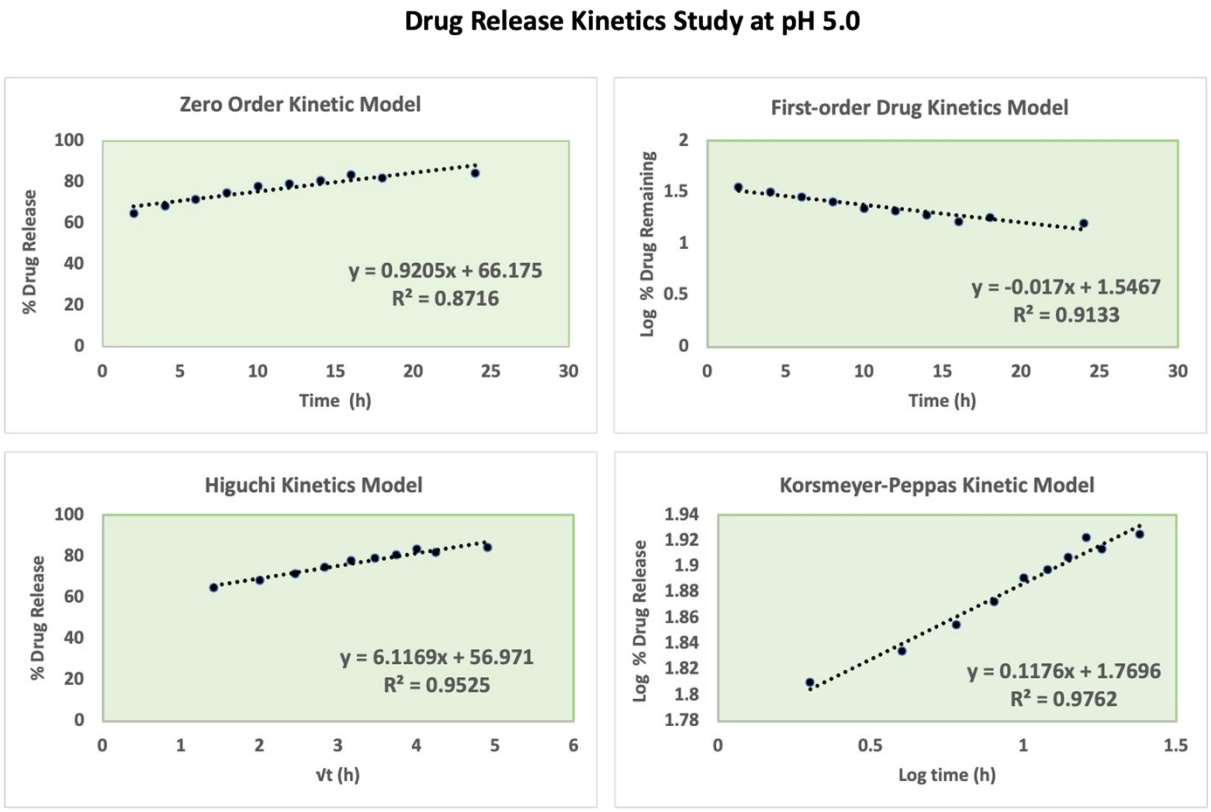

Figure S7. Linear regression plots for drug release kinetics models. (a) Zero-order kinetic model plotted as cumulative percent drug released (%DR) versus time. (b) First-order kinetic model plotted as log(% drug remaining) versus time. (c) Higuchi kinetic model plotted as %DR versus the square root of time (√t). (d) Korsmeyer–Peppas kinetic model plotted as log(%DR) versus log(time). The DR kinetic modeling was performed for pH 5.0

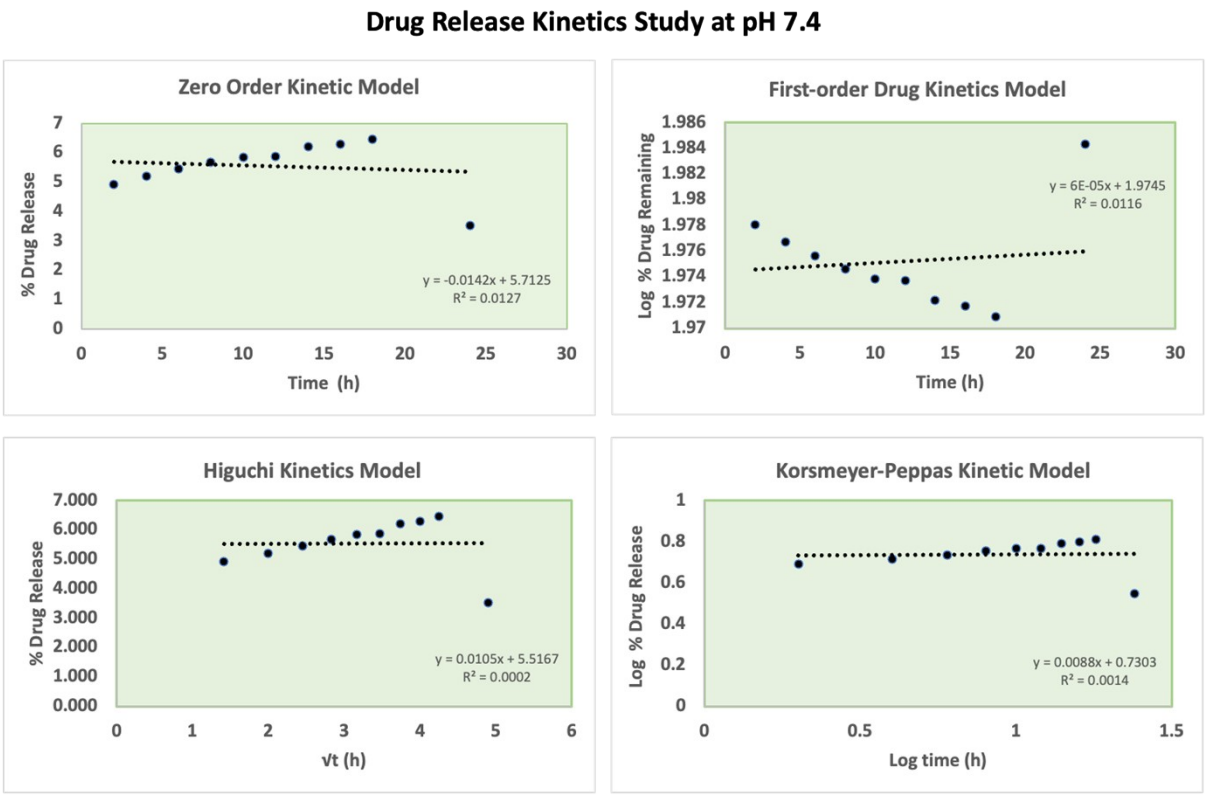

Figure S8. Linear regression plots for drug release kinetics models. (a) Zero-order kinetic model plotted as cumulative percent drug released (%DR) versus time. (b) First-order kinetic model plotted as log(% drug remaining) versus time. (c) Higuchi kinetic model plotted as %DR versus the square root of time (√t). (d) Korsmeyer–Peppas kinetic model plotted as log(%DR) versus log(time). The DR kinetic modeling was performed for pH 7.4

Drug Release Kinetics Analysis. The drug release from the formulation was studied at pH levels of 5.0 and 7.4 to evaluate the effect of the medium on the release mechanism. Linear regression was applied to four kinetic models—zero-order, first-order, Higuchi, and Korsmeyer–Peppas. At pH 5.0, the correlation coefficients (R^2) were 0.87, 0.91, 0.95, and 0.976, respectively. The zero-order and first-order models showed moderate linearity, indicating that the release was not constant and depended on the remaining drug concentration. The Higuchi model showed good agreement, suggesting diffusion-controlled release, while the Korsmeyer–Peppas model provided the best fit (R^2 = 0.976). The release

exponent (n = 0.12) confirmed a Fickian diffusion mechanism, indicating that the drug diffused through the polymeric network at a controlled rate. At pH 7.4, all models exhibited very low correlation ($R^2 < 0.02$), indicating almost no measurable release over time. This behavior suggested that the matrix remained intact, preventing drug diffusion, likely due to reduced polymer relaxation or limited solvent penetration at physiological pH. Overall, the results demonstrated that the drug release was pH-dependent, being diffusion-driven and significant at pH 5.0, but minimal at pH 7.4. The Korsmeyer–Peppas model best described the release behavior under acidic conditions, confirming a Fickian diffusion mechanism.

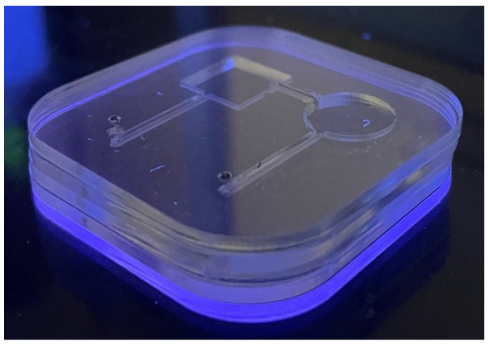

Figure S9. Photograph of the fabricated PMMA-based microfluidic chip bonded using a pressure-sensitive adhesive (PSA) tape. The device features a single-chamber microchannel design with inlet and outlet ports and a circular well for hydrogel placement. The transparent PMMA layers and PSA bonding ensured leak-free sealing while allowing optical observation and controlled fluid flow for in vitro drug-release studies.

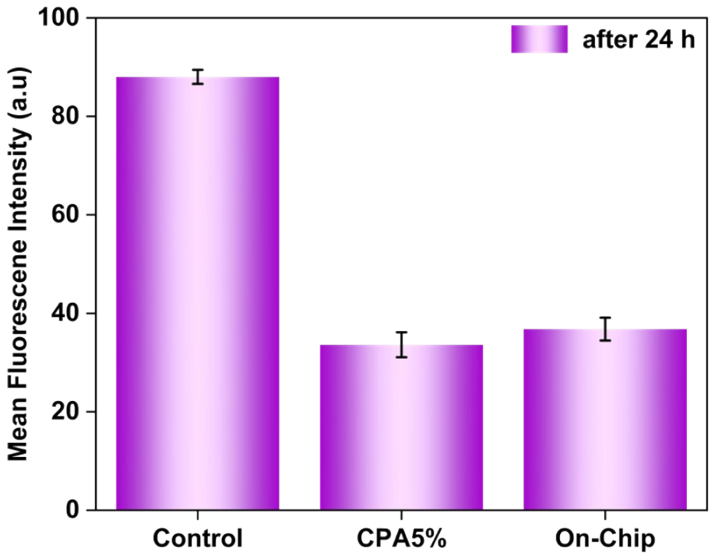

Figure S10. Mean fluorescence intensity (MFI) of viable A498 renal carcinoma cells stained with acridine orange (AO) after 24 h of incubation under different conditions: control (Plastic-substrate), CPA5% hydrogel, and CPA5% hydrogel on-chip system. Data are presented as mean ± SD (n = 3).

Possible Explanation to the best of our knowledge: The mean fluorescence intensity (MFI) of acridine orange (AO)–stained A498 cells was used to assess relative cell viability under different culture configurations (Figure S7). The control (2D) group exhibited the highest MFI, which was attributed to the uniform monolayer growth of cells that occupied a larger illuminated surface area and produced stronger fluorescence emission. In contrast, cells grown within the Soft CPA5% Hydrogel substrate and on-chip systems displayed lower MFI values. This reduction was not solely due to decreased cell viability but also reflected the formation of compact spheroids and the three-dimensional spatial organization of cells within the hydrogel matrix. The embedded architecture limited light penetration and dye diffusion, thereby attenuating fluorescence intensity. These observations confirmed that the CPA5% hydrogel and microfluidic chip provided a physiologically relevant soft hydrogel-supported

3D-like renal tumor model, where cell organization and optical signal characteristics differed markedly from those in conventional 2D culture.

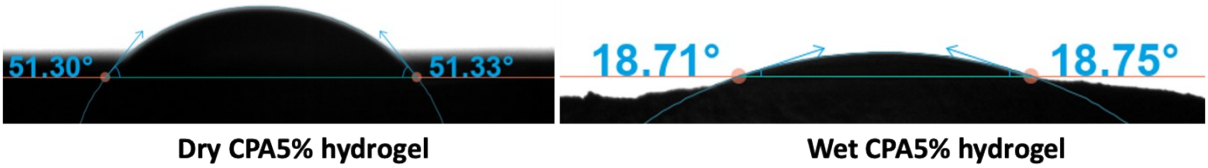

Figure S11. Water contact angle measurements of CPA5% hydrogels showing surface wettability differences between dry and hydrated hydrogel (a) The dried CPA5% hydrogel exhibited a contact angle of ~51°, indicating moderate hydrophilicity. (b) After swelling, the contact angle decreased to ~18°, confirming enhanced surface hydrophilicity due to exposure of polar –OH and –COOH groups. The increased wettability facilitates better fluid absorption and cell adhesion, beneficial for biological and drug delivery applications.

Table S1. Summary of Composition of CPA based Hydrogel.

S.No	Polymer matrix	Conc. (W/V)%	Mixing Ratio
1	Na-CMC/PVA/ Agarose 1 % (CPA 1%)	2 % -Na-CMC 10% PVA 1% Agarose	1:1:1
2	Na-CMC/PVA/ Agarose 2 % (CPA 2%)	2 % -Na-CMC 10% PVA	1:1:1

		2% Agarose	
3	Na-CMC/PVA/ Agarose 3 % (CPA 3%)	2 % -Na-CMC 10% PVA 3% Agarose	1:1:1
4	Na-CMC/PVA/ Agarose 4 % (CPA 4%)	2 % -Na-CMC 10% PVA 4% Agarose	1:1:1
5	Na-CMC/PVA/ Agarose 5 % (CPA 5%)	2 % -Na-CMC 10% PVA 5% Agarose	1:1:1

References:

1. H.-F. Tsai, A. Trubelja, A. Q. Shen and G. Bao, *J. R. Soc. Interface*, 2017, **14**, 20170137.
2. P. M. Arvejeh, F. A. Chermahini, F. Marincola, F. Taheri, S. A. Mirzaei, A. Alizadeh, F. Deris, R. Jafari, N. Amiri and A. Soltani, *J. Transl. Med.*, 2025, **23**, 382.
3. H. Hanan, F. Pervaiz, M. Ijaz, S. M. Javaid, A. N. Bukhari, T. Arshad, S. J. Akhtar and A. Majeed, *J. Drug Deliv. Sci. Technol.*, 2024, **92**, 105358.
4. J. Yuan, W. Sun, Z. Zhang, Y. Wang, D. Huang, D. Ren, H. Chen, X. Wang, G. Li and Z. Han, *Biomater. Adv.*, 2025, **168**, 214108.
5. S. Khan, B. Khan and H. Li, *Beni-Suef Univ. J. Basic Appl. Sci.*, 2023, **12**, 117.
6. M. Arslan, M. U. Ashraf, A. M. Al-Qaaneh, A. Aslam, A. Mahmood, H. Ijaz, R. M. Sarfraz, M. M. Salem, M. A. Mezher and M. M. Bekhit, *AAPS PharmSciTech*, 2025, **26**, 132.
7. Y. Ye, W. Wang, X. Liu, Y. Chen, S. Tian and P. Fu, *Gels*, 2023, **10**, 21.
8. Y. Shintani, H. Katagiri and M. Ikeda, *Adv. Funct. Mater.*, 2024, **34**, 2312999.
9. M. I. Calafel, M. Criado-Gonzalez, R. Aguirresarobe, M. Fernández and C. Mijangos, *Mater. Adv.*, 2025, **6**, 4566–4597.
10. F. L. C. Morgan, I. A. O. Beeren, L. Moroni and M. B. Baker, *Chem. Mater.*, 2025, **37**, 2709–2719.
11. H. Jongprasitkul, S. Turunen, M. Kellomäki and V. S. Parihar, *Mater. Adv.*, 2024, **5**,

5823–5837.

12. Y. Zhou, F. Dai, S. Zhao, Z. Li, H. Liang, X. Wang, L. Zhao and H. Tan, *Adv. Healthc. Mater.*, 2025, 2500810.
13. K. Kowalczuk, V. D. Wegner, A. S. Mosig and F. H. Schacher, *ACS Appl. Bio Mater.*, 2024, **7**, 2402–2412.
14. S. Lambrecht, H. Schröter, H. Pohle and S. Jopp, *ACS omega*, 2024, **9**, 5418–5428.
15. W. Feng and Z. Wang, *Adv. Sci.*, 2023, **10**, 2303326.
16. Y. Leng, C. N. Britten, F. Tarannum, K. Foley, C. Billings, Y. Liu and K. B. Walters, *ACS omega*, 2024, **9**, 37687–37701.
17. H. Lan, Y. Zhang, Z. Dong and X. Zhang, *Mater. Des.*, 2025, 114103.
18. M. J. Dehghan-Nayeri, F. Peytam, A. Foroumadi and M. Mahdavi, *Sci. Rep.*, 2025, **15**, 20852.